Nano Energy (▮▮▮▮) ▮, ▮▮▮–▮▮▮

Available online at www.sciencedirect.com

ScienceDirect

journal homepage: www.elsevier.com/locate/nanoenergy

RAPID COMMUNICATION

A general strategy for the fabrication of high performance microsupercapacitors

Q1 Narendra Kurra, Qiu Jiang, H.N. Alshareef

Q3 Q2 *Materials Science and Engineering, King Abdullah University of Science and Technology (KAUST), Thuwal 23955-6900, Saudi Arabia*

Received 1 April 2015; received in revised form 12 May 2015; accepted 25 May 2015

KEYWORDS
Micropseudocapacitors;
Heterostructures;
Reduced graphene oxide;
Conducting polymer;
In-plane

Abstract

We propose a generic strategy for microsupercapacitor fabrication that integrates layers of reduced graphene oxide (rGO) and pseudocapacitive materials to create electrode heterostructures with significantly improved cycling stability and performance. Our approach involves a combination of photolithography and a simple transfer method of free-standing reduced graphene oxide film onto an Au/patterned photoresist bilayer. The resulting stack (rGO/Au/patterned resist/substrate) is then used for the electrochemical deposition of various pseudocapacitive materials before the final step of lift-off. To prove the viability of this method, we have successfully fabricated microsupercapacitors (MSCs) with the following interdigitated electrode heterostructures: MnO_2/rGO, $Co(OH)_2$/rGO and PANI/rGO. These MSCs show better performance and cycling stability compared to the single layer, (i.e., rGO-free) counterparts. The interdigitated electrode heterostructures result in MSCs with energy densities in the range of 3–12 mW h/cm^3 and power densities in the range of 400–1200 mW/cm^3, which is superior to the Li thin film batteries (E=10 mW h/cm^3), carbon, and metal oxide based MSCs (E=1–6 mW h/cm^3) while device energy densities are in the range of 1.3–5.3 mW h/cm^3, corresponding power densities are in the range of 178–533 mW/cm^3. These results can be explained by a facilitated nucleation model, where surface topology of the rGO film creates a favorable environment for the nucleation and growth of pseudocapacitive materials with strong interfacial contacts and enhanced surface area. This approach opens up a new avenue in fabricating MSCs involving a variety of heterostructures combining electrical double layer carbon type with Faradaic pseudocapacitive materials for enhanced electrochemical performance.

E-mail address: husam.alshareef@kaust.edu.sa (H.N. Alshareef).

http://dx.doi.org/10.1016/j.nanoen.2015.05.031
2211-2855/

Introduction

The next generation of energy storage devices is expected to include devices fabricated in the planar format due to their compatible integration with microelectronic devices [1-3]. This reality has fostered the rapid development of on-chip energy storage devices such as thin film batteries and microsupercapacitors (MSCs) [4-7]. MSCs have become attractive owing to their high power densities and longer cycle life compared to thin film batteries, which suffer from poor rate capability and limited cycle lifetimes [4,6]. Additionally, due to their planar configuration, MSCs can exhibit higher charge-discharge rates compared to their conventional counterparts [6,7].

High surface area porous carbon based MSCs such as carbide derived [8], onion like[9], activated [10] and carbon nanotubes (CNTs) [11] were fabricated by employing conventional photolithography and various deposition methods including sputtering, electrophoretic, ink-jet printing and spray coating techniques. Further, conducting graphitic patterns involving 2D graphene and 1D CNTs were grown by chemical vapor deposition (CVD) to fabricate three-dimensional MSCs [12,13]. Of late, reduced graphene oxide (rGO), due to its high surface area, conductivity and functionality, has become an attractive material for energy storage applications [14,15]. For example, Gao et al., have used laser reduction to write reduced graphene oxide patterns over the GO thin films in order to fabricate rGO MSCs [16]. El-Kady et al., have demonstrated scalable fabrication of rGO MSCs by ordinary digital video disk (DVD) laser scribing technique [17]. Wu et al., have employed photolithography and oxygen plasma to create rGO based micropatterns and further demonstrated electrochemical performance of these MSCs [18]. As the mechanism of charge storage in these carbonaceous materials is of non-Faradaic type, these MSCs exhibited limited values of capacitance. Hence, in order to improve the capacitance values, pseudocapacitive materials such as metal oxides/hydroxides (RuO_2, MnO_2 and $Ni(OH)_2$) [19-21] and even conducting polymers (PPY, PANI) [22-24] which can undergo reversible redox reactions at their surfaces have been employed to fabricate micro-pseudocapacitors. However, pseudocapacitive materials suffer from poor cycling performance, which has been circumvented through the fabrication of hybrid electrodes composed of composites of rGO with pseudocapacitive materials [25-27]. The complimentary roles between these two components have been exploited where reduced graphene oxide serves not only as a conducting network for facile charge transport, but also as a mechanical support in improving cycling stability of these hybrid electrodes. Recently, there have been efforts in fabricating pseudocapacitive/reduced graphene oxide electrode heterostructures employing micromolding and filtration methods [28,29].

Patterning of pseudocapacitive/rGO heterostructures is of significant interest for achieving better electrochemical performance of MSCs. Here, we propose a simple and generic strategy for the fabrication of pseudocapacitive/rGO planar microsupercapacitor devices using a single step photolithography process. Free standing rGO films, obtained through vacuum filtration process, are transferred onto substrates having metal-coated patterned photoresist layer. The resulting stack (rGO/metal/patterned resist/substrate) is selectively coated by metal oxides (MnO_2 and $Co(OH)_2$) and conducting polymer (PANI) over the transferred rGO layer, followed by lift-off process. The result is a MSC with interdigitated patterns of different pseudocapacitive materials on rGO. As microsupercapacitor is comprised of a few microns thick film, electrochemical deposition can be a facile method, resulting in the mesoporous morphology of pseudocapacitve materials, required for maximum accessible surface area for the electrolyte ions. Avoiding binders or additives, while maintaining good interfacial contact through electrochemical deposition, ensures strong adherence with current collectors, helps in facile electron transfer across the pseudocapacitive/current collector interface. This in-plane design of hybrid electrodes with no separator ensures facile transport of ions, resulting in high scan rate abilities of heterostructured microsupercapacitor with improved cycling stability.

Experimental

Photolithography

Glass substrates (Fisher) were cut into 1 × 1 in. size, cleaned with a soap solution to remove the dirt followed by ultrasonication in acetone, isopropanol and deionized water sequentially for 5 min each and then dried by blowing nitrogen. Photoresist AZ9260 was spun coated at 3000 rpm for 60 s over the glass substrates to get 10 μm thick photoresist layer. Photoresist coated substrates were soft baked at 110 °C for 3 min. The exposure was done using EVG contact aligner at a constant dose of 1800 mJ/cm^2 through the Cr/Glass mask having the interdigitated patterns. After the exposure, samples were developed in AZ726 developer solution for 6 min, which has resulted in the formation of patterns in the photoresist layer. Metal layers of 200 nm Au/20 nm Ti were deposited by sputtering (Equiment Support Co., Cambridge, England) technique over the patterned photoresist layer. Before the lift-off process, rGO layer was transferred onto metal-coated patterned photoresist followed by electrodeposition of pseudocapacitive materials. In this study, we have employed interdigitated finger electrodes (width of each finger 100 μm, and spacing between the fingers is 50 μm); the total area of all the fingers is 0.25 cm^2.

RGO preparation and filtration

Graphite oxide was prepared from natural graphite source using a modified Hummers method [30]. Thus obtained graphite oxide was exfoliated in de-ionized (DI) water by sonicating using a bath sonicator (UP400S, Ultrasonic processor; Hielscher ultrasound Technology) for 1 h. The resulting graphene oxide was then reduced to graphene by following the method that was reported by Li et al. [31] Briefly, the homogeneous graphene oxide dispersion (5.0 mL) was mixed with 5.0 mL of water, 5.0 μL of hydrazine solution (35 wt% in water) and 100.0 μL of ammonia solution (28 wt% in water). The optimal hydrazine to graphene oxide weight ratio was 7:10 [31,32]. The mixture

Please cite this article as: N. Kurra, et al., A general strategy for the fabrication of high performance microsupercapacitors, Nano Energy (2015), http://dx.doi.org/10.1016/j.nanoen.2015.05.031

was then stirred at 95 °C for 1 h followed by centrifugation at 10,000 rpm for 30 min to remove flocculated graphene. The supernatant solution containing thin layers of rGO was used for obtaining free-standing rGO films. The rGO dispersion was filtered using vacuum filtration (VF) method on a porous alumina membrane filter (0.2 μm pore size and 25 mm diameter; Whatman). The alumina membrane was removed by dissolving it into a bath of 3 M NaOH solution in order to obtain free-standing rGO film. This film was then transferred to a water bath to remove the traces of adsorbed NaOH over the rGO surface and this step was repeated for several times. Finally, rGO film (thickness, 50 nm) was transferred onto the Au-coated patterned photoresist chip followed by drying off in a heating oven at 60 °C for 3 min. Various pseudocapacitive materials were electrodeposited over the rGO films (thickness 0.1–1 μm). Typical mass loading of active materials was found to be less than 1 mg/cm^2, we have estimated the electrochemical performance in terms of area and volume of the electrodes as gravimetric values may get overestimated [6].

Electrochemical deposition of MnO_2 electrodes on rGO

All reagents in the experiment are of analytical grade, which were used as received without further treatment. Electrochemical deposition was performed in a three-electrode configuration employing either rGO/Au or Au film coated on patterned photoresist substrates as the working electrode, Pt wire and Ag/AgCl as counter and reference electrodes, respectively. The electrochemical deposition of MnO_2 was carried out by employing 10 mM of $Mn(NO_3)_2$ with 50 mM of $NaNO_3$ as a supporting electrolyte [33]. Galvanostatic deposition technique with a constant current density of 0.5 mA/cm^2 was applied using an electrochemical workstation (CH Instruments 660D). After the electrodeposition process, the samples were thoroughly washed with DI water to remove the unreacted precursor. The samples were dried by blowing nitrogen followed by lift-off using acetone to obtain the MnO_2/rGO or MnO_2 interdigitated electrodes.

Electrochemical deposition of $Co(OH)_2$ electrodes on rGO

$Co(OH)_2$ was electrodeposited employing 5 mM $Co(NO_3)_2 \cdot 6H_2O$ aqueous electrolyte at a constant potential of −1 V (vs. SCE) [34]. The thickness of the deposit was controlled through the plating time. After the electrodeposition process, the electrode substrate was carefully rinsed several times with deionized water followed by drying using N_2 gas.

Electrochemical deposition of PANI electrodes on rGO

PANI was electrodeposited employing 100 mM aniline+0.75 M H_2SO_4 as an electrolyte by applying a constant potential of 0.8 V for 2 min as a nucleation layer followed by galvanostatic deposition at a constant current of 0.5 mA/cm^2 to grow PANI nanowires [35].

Material characterization

Surface morphology and microstructure were imaged by scanning electron microscope (SEM) (Nova Nano 630 instrument, FEI Co., The Netherlands). The film thicknesses were measured using a Veeco Dektak 150 surface profilometer. Raman spectroscopy measurements were carried out on the samples using a micro-Raman spectrometer (LabRAM ARAMIS, Horiba-Jobin Yvon). Raman spectra acquired with notch filters cutting at 100 cm^{-1} using a Cobalt laser (473 nm, 5 mW at source) and a laser spot size of 1.5 μm.

Electrochemical measurements

The electrochemical performance of MSCs with different pseudocapacitive materials/rGO electrodes was investigated in a 2-electrode configuration using an electrochemical workstation (CHI 660D, CH Instruments Incorporation). Cyclic voltammetry (CV), galvanostatic charge–discharge (CD), and electrochemical impedance spectroscopy (EIS) measurements were carried out. The electrolytes used including 1 M Na_2SO_4 in the case of MnO_2, 1 M KOH for $Co(OH)_2$ and 1 M H_2SO_4 for PANI MSCs. Solid state devices were made by employing gel electrolytes such as Polyvinyl alcohol (PVA)/KOH and PVA/H_2SO_4. PVA/KOH gel electrolyte was prepared by mixing 1.2 g of KOH with 2 g of PVA in 20 mL of water followed by rigorous stirring at 85 °C until the formation of a clear gel. Similarly, The PVA/H_2SO_4 gel electrolyte was prepared as follows: 1 g of H_2SO_4 was added into 10 mL of deionized water, followed by 1 g of PVA powder. The whole mixture was heated to 85 °C while stirring until the solution became clear. Solid-state devices were fabricated by dropping 10 μL of the gel electrolyte across the finger electrodes followed by drying at room temperature. CV experiments were carried out at different scan rates selected from 0.01 to 100 V/s. CD experiments were performed using current densities selected from 40 to 250 μA/cm^2. EIS experiments were carried out at a direct current (DC) with 0 V bias and a sinusoidal signal of 5 mV in a frequency range from 0.1 Hz to 100 kHz. All measurements were done at room temperature (22±1 °C).

Results and discussion

The schematic shown in Figure 1 depicts the fabrication of pseudocapacitive/rGO interdigitated electrodes by employing conventional photolithography followed by rGO layer transfer, electrochemical deposition of pseudocapactive materials, and finally resist lift-off. The initial photolithography process involved spin coating of positive photoresist followed by exposure to UV light through a Cr mask. The resist layer was then developed to obtain interdigitated patterns as shown in Figure 1a. Now, the patterned photoresist layer was coated with Au/Ti metal layers, as shown in Figure 1b. Thin films (thickness, 50 nm) of rGO were obtained through vacuum filtration over the porous alumina membrane, as shown in Figure 1c. These membranes were then dissolved away in NaOH solution to obtain freely-floating rGO films over the water bath. These rGO films (as described in the *Experimental section*, see also Figures S1 and S2, Supplementary materials) were then transferred onto the

Please cite this article as: N. Kurra, et al., A general strategy for the fabrication of high performance microsupercapacitors, Nano Energy (2015), http://dx.doi.org/10.1016/j.nanoen.2015.05.031

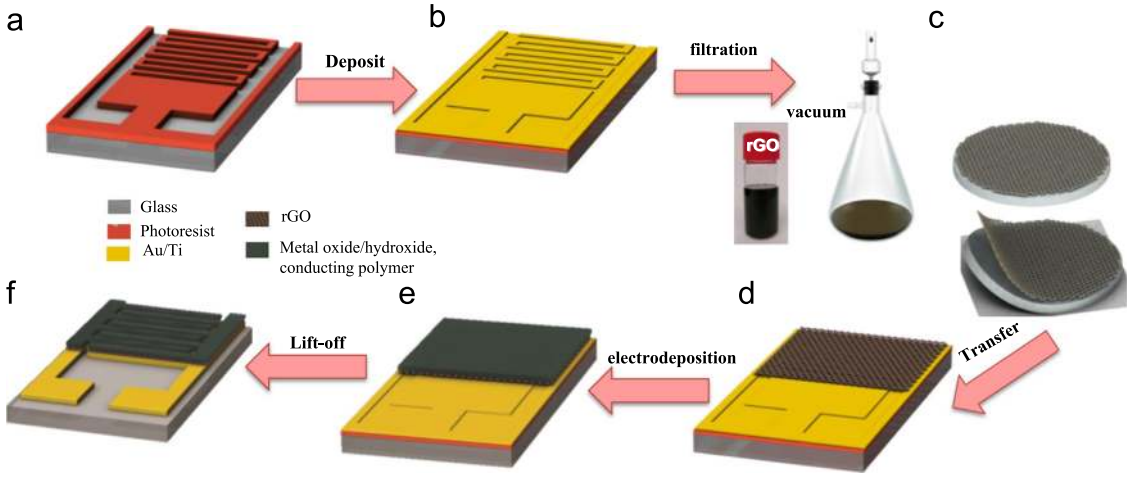

Figure 1 Schematic illustrating the fabrication process of microsupercapacitors with rGO based heterostructures. (a) Patterned photoresist layer, (b) metal deposition, (c) vacuum filtration of rGO thin film over alumina membrane, (d) fishing of rGO thin film over the metal coated patterned photoresist substrate, (e) electrochemical deposition of pseudocapacitive materials over the rGO surface, (f) lift-off in acetone to obtain interdigitated finger electrodes with pseudocapacitive/rGO heterostructures.

patterned area of the metal-coated photoresist, as shown in Figure 1d. Furthermore, pseudocapacitive materials such as metal oxides/hydroxides (MnO_2 and $Co(OH)_2$) and conducting polymer, PANI, were electrodeposited over the stack of rGO/metal/patterned photoresist/substrate, as shown in Figure 1e. The final step of lift-off process results in the formation of interdigitated fingers of pseducapacitive/rGO electrodes, while dissolving away unexposed photoresist as shown in Figure 1f. This unique strategy helped us in obtaining uniform growth of pseudocapacitive materials over the rGO layer in a single run of photolithography process. Lift-off process as the final step gave rise to the neat interdigitated finger electrodes comprised of pseudocapacitive coatings over the rGO patterns. These hybrid electrodes in the in-plane configuration indeed exhibited good electrochemical performance as discussed below.

The versatile nature of rGO platform in terms of chemical functionality and conductivity helps in the homogeneous nucleation and growth of pseudocapacitive materials. It was observed that the rGO film obtained through the filtration process is comprised of tightly packed rGO sheets (lateral dimensions are in the order of a few hundreds of nanometers) with local protrusions (see Figure S2d, Supplementary materials). Thus, rGO film is encompassed of a myriad of surface-steps, domain boundaries, and interfaces which we believe are favorable for the nucleation and growth of pseudocapacitive materials with morphologies having very good electrochemical performance. The morphologies of electrodeposited MnO_2, $Co(OH)_2$ and PANI materials over the rGO films are shown in Figure 2. As shown in Figure 2a and b, the growth morphology of MnO_2 and $Co(OH)_2$ consist of interconnected vertical petals (width and height of the petals was found to be 0.1 and 0.5 μm, respectively) with mesoporous morphology, which can facilitate the rapid movement of electrolyte ions (see Figure S3, Supplementary materials). Electrochemical deposition of PANI was done in a two-step electrodeposition in which initial nucleation of PANI film at a constant potential followed by out-of-plane growth resulting in spiky-type morphology as shown in Figure 2c. The attachment of pseudocapacitive material to the rGO film is as strong as they could sustain ultra-sonication during the final step of lift-off. Thus, the intimate interfacial contact between the pseudocapacitive materials and the rGO platform ensures good chemical and mechanical stability, which further affects the electrochemical performance of these rGO based heterostructured electrodes.

Raman spectra for the electrodeposited pseudocapacitive materials over the rGO film were shown in Figure 2d. The broad peaks at 1366 and 1595 cm^{-1} are assigned to the D (FWHM, 197.8 cm^{-1}) and G (FWHM, 90.9 cm^{-1}) bands of rGO [36]. The D band is due to defects and is related to zone boundary k-point phonons with A_{1g} symmetry while the G band corresponds to symmetric stretching of sp^2 carbon lattice with E_{2g} symmetry [37-39]. The I_D/I_G ratio of rGO films was found to be 0.84, corresponds to the sp^2 crystallite size of 14.3 nm, estimated using the following formula [39]:

$$L_a(\mathrm{nm}) = 560/E_{\mathrm{laser}}^4 \left(I_D/I_G\right)^{-1} \quad (1)$$

where E_{laser} is the laser excitation energy in eV.

The Raman spectrum shows bands at 171, 260, 392, 573 and 638 cm^{-1}, which correspond to β-MnO_2 (see black spectrum in Figure 2d). The first three bands may correspond to the deformation modes of the metal-oxygen chain of Mn-O-Mn, and the bands at 573 and 638 cm^{-1} correspond to the stretching mode of the Mn-O lattice [40]. The Raman spectrum for $Co(OH)_2$/rGO is shown as red curve in Figure 2d. The peaks at lower wave numbers 193, 472, 511, 603 and 672 cm^{-1} correspond to E_g, F_{m1}^2, F_{2g}^2 and A_{1g} modes of $Co(OH)_2$ [41-43]. Similarly, the blue spectrum shown in Figure 2d corresponds to electrodeposited PANI over rGO film. The bands at 1623 and 1529 cm^{-1} can be assigned to C=C and C=N stretching vibrations, bands at 827 and 415 cm^{-1} correspond to C-H deformation while bands at 1396, 1340, 1262, 1195, 741, 574 and 514 cm^{-1} are related to benzene ring deformations [44]. The stretching vibrations of C=C and benzene ring deformations of PANI overlap with that of D and G bands of rGO (see blue spectrum in Figure 2d).

Please cite this article as: N. Kurra, et al., A general strategy for the fabrication of high performance microsupercapacitors, Nano Energy (2015), http://dx.doi.org/10.1016/j.nanoen.2015.05.031

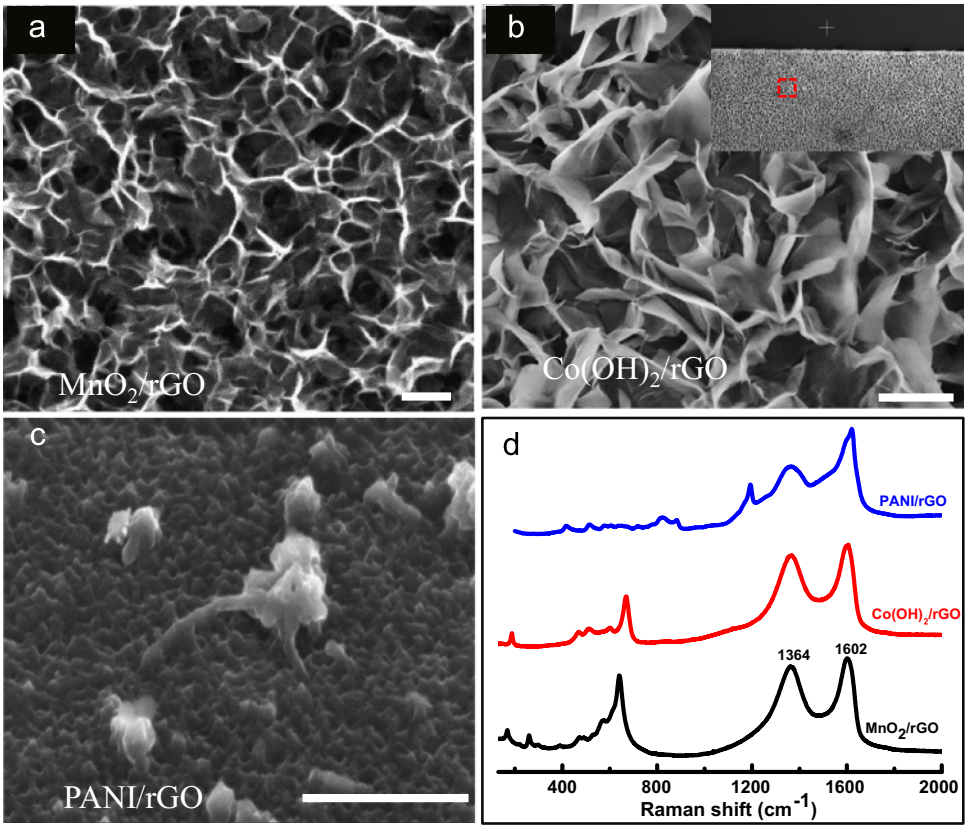

Figure 2 (a)-(c) SEM micrographs of MnO_2, $Co(OH)_2$ and PANI grown over rGO layer, inset shows the interdigitated finger electrodes. Scale bar, 1 μm. (d) Representative Raman spectra of pseudocapacitive/rGO films.

Electrochemical performance of MnO_2/rGO MSC was investigated in 1 M Na_2SO_4 in a 2-electrode configuration. Optimal specific capacitance of the various pseudocapacitive materials was estimated using 3-electrode configuration (see Figure S4, Supplementary materials). The CV curves shown in Figure 3a reveal that MnO_2/rGO MSC exhibit 1.5 times higher values of current when compared to MnO_2/Au MSC at a given scan rate of 10 V/s. The rGO only MSCs exhibit an areal capacitance of 0.12 mF/cm^2, a negligible contribution towards the capacitance shown by MnO_2/rGO hybrid electrode (see Figure S5, Supplementary materials). The enhanced values of capacitance can be attributed to the morphology of MnO_2 grown over the rGO film compared to Au metal surface. It has been demonstrated that composites of rGO with metal oxides can have enhanced electrochemical performance due to synergistic interactions between these components [45]. Further, it has been shown that the chemical functional groups on rGO ensure strong interfacial contacts with metal oxides and provides a medium for efficient charge transfer ability, enhancing the capacitance of this hybrid electrode [25]. As shown in Figure 3b, the CV curves are quite rectangular up to the high scan rates of 20 V/s. Reversible Faradaic reactions at the surface of MnO_2 electrodes contribute to the observed pseudocapacitance besides the negligible contribution from the double layer capacitance of rGO [45]. A possible mechanism for the pseudocapacitance of MnO_2 can be described by the following Faradaic reaction:

$$MnO_2 + Na^+ + e^- \leftrightarrow MnOONa \quad (II)$$

As the Mn ions vary between III and IV oxidation states due to fast reversible Faradaic reactions, they result in nearly ideal capacitive behavior. Charge-discharge curves are also rather linear at different current densities, as shown in Figure 3c. The areal capacitance of the MnO_2/rGO MSC was found to be 2.1 mF/cm^2 at a current density of 65 μA/cm^2, which is almost 1.5 times higher than MnO_2 only MSC. The variation in the volumetric capacitance with current density is shown in Figure 3d. The volumetric capacitance was calculated by dividing the areal capacitance with thickness of the electrode (0.55 μm) and found to be 38 F/cm^3 at a current density of 65 μA/cm^2. Nyquist plots of MnO_2/rGO and MnO_2/Au MSCs are shown in Figure 3e. The high frequency portion of the impedance spectra show a small semi-circle, indicating the existence of charge-transfer resistance while in the low frequency region, the vertical nature of the curve for the MnO_2/rGO indicates a dominant capacitive behavior. The cycling stability of both MSCs were tested by continuous charging and discharging over 10,000 cycles, as shown in Figure 3f. In the case of metal oxide-rGO microsupercapacitor (MSC), capacitance retention of 77% was observed for initial 5000 cycles while it was only 26% for the metal oxide microsupercapacitor (without rGO). For the last 5000 cycles, the capacitance fading in the case of metal oxide/rGO MSC was negligible with only 8% fading. While in the case of MnO_2 MSC, capacitance fading of 17% was observed for the last 5000 cycles. Overall, after 10,000 cycles MnO_2/rGO MSC could retain the capacitance up to 69% when compared to the retention of only 9% for the MnO_2 MSC (without rGO). Further, we have examined the

Please cite this article as: N. Kurra, et al., A general strategy for the fabrication of high performance microsupercapacitors, Nano Energy (2015), http://dx.doi.org/10.1016/j.nanoen.2015.05.031

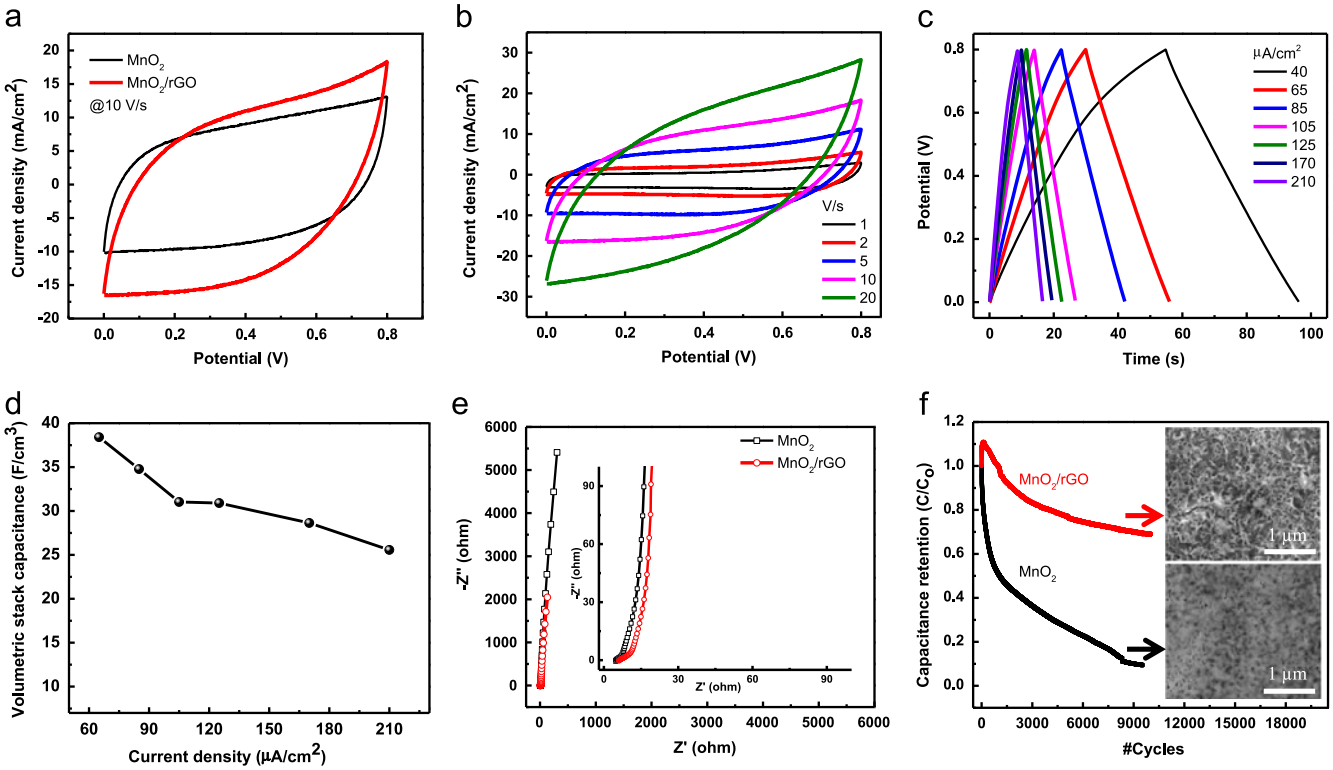

Figure 3 Electrochemical performance of MnO_2/rGO MSC. (a) Comparative CVs of MnO_2 and MnO_2/rGO MSCs at a scan rate of 10 V/s. (b) CVs and (c) CDs of MnO_2/rGO MSC in 1 M Na_2SO_4 electrolyte. (d) Volumetric stack capacitance with current density. (e) Nyquist spectra of MnO_2 and MnO_2/rGO MSCs, inset showing the high frequency region of the spectra. (f) Cycling stability of MnO_2 and MnO_2/rGO MSCs over 10,000 cycles by charging and discharging continuously at a current density of 105 μA/cm^2. Inset shows SEM micrographs for MnO_2/rGO and MnO_2/Au after the cycling test.

electrode morphology after the cycling test and the SEM images are provided in the inset of Figure 3f. It appears that the dissolution of MnO_2 was relatively faster on Au surface when compared to the rGO nucleation layer during cycling test. Hence, we believe that the rGO layer helps in suppressing the dissolution rate of metal oxides during cycling test, enabling us to fabricate relatively stable micro-pseudocapacitors. It can be anticipated that rGO could help in suppressing the volume change, agglomeration and dissolution of metal oxides during the cycling, leading to improved cycling stability of the hybrid device [25,26].

Cobalt hydroxide ($Co(OH)_2$) is a layered material which exhibit characteristic redox reactions with a high theoretical specific capacitance up to 3500 F/g, making it a potential pseudocapacitive material in hybrid electrodes [44,45]. During electrodeposition, the local change of pH due to generation of hydroxyl ions (OH^-) at the rGO surface facilitates the growth of $Co(OH)_2$ in form of interconnected vertically oriented sheets (see Figure 4a). This particular morphology is good due to enhanced $Co(OH)_2$ surface area, which is accessible to Faradaic reactions, significantly contribute to the higher values of capacitance. The electrochemical performance of $Co(OH)_2$/rGO MSCs were investigated in 1 M KOH in 2-electrode configuration. The pseudocapacitive behavior of $Co(OH)_2$ was evident from the appearance of redox peaks at different scan rates, as shown in Figure. 4b and c. The redox peaks correspond to oxidation of $Co(OH)_2$ to CoOOH and reverse reaction that happen during the reduction process [46]. Thus, the Faradaic behavior of $Co(OH)_2$ can be due to the following plausible reaction as a quasi-reversible redox process during the potential sweep of the film electrode [14,38]:

$$Co(OH)_2 + OH^- \leftrightarrow CoOOH + H_2O + e^- \quad \text{(III)}$$

The redox behavior was observed up to a scan rate of 20 V/s, as shown in Figure 4c. This high scan rate capability can be attributed to the interdigitated electrode architecture which can facilitate easy transport of electrolyte ions even at higher scan rates. As shown in Figure 4d, the cathodic and anodic peak current densities vary linearly with the square root of scan rate, indicating diffusion controlled redox reactions, unlike the MSCs based on carbonaceous materials [8,9,46]. Similarly, charge-discharge curves were recorded at different current densities and they show non-linear behavior, due to pseudocapacitive behavior of $Co(OH)_2$ (see Figure 4e). The areal capacitance was found to be 6 mF/cm^2 at a current density of 65 μA/cm^2 which corresponds to a volumetric capacitance of 119 F/cm^3. Solid state MSCs were made by employing PVA/KOH gel electrolyte (see Figure S6, Supplementary materials). This device shows an areal capacitance of 2.7 mF/cm^2 (corresponding volumetric capacitance of 54 F/cm^3), value is almost two times lower compared to liquid electrolyte. It seems that gel electrolyte may not be able to access the

Please cite this article as: N. Kurra, et al., A general strategy for the fabrication of high performance microsupercapacitors, Nano Energy (2015), http://dx.doi.org/10.1016/j.nanoen.2015.05.031

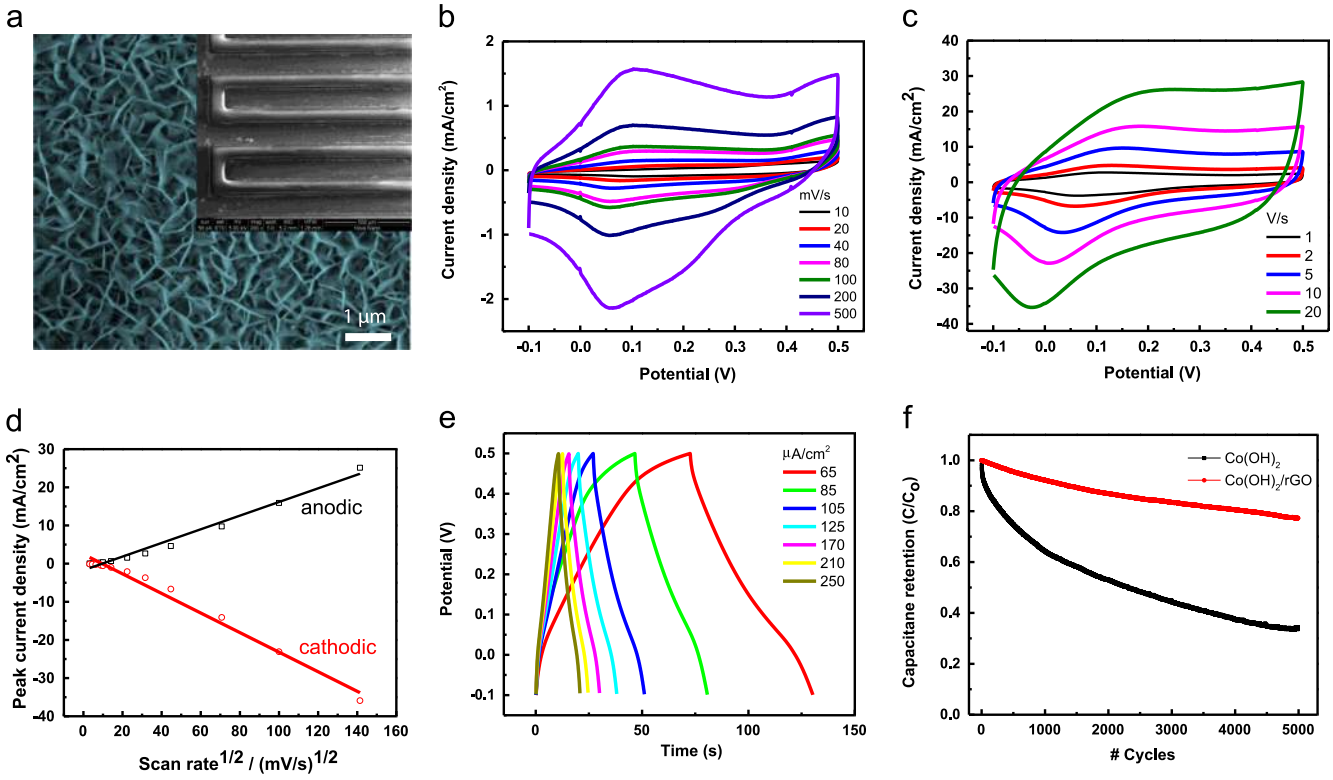

Figure 4 (a) SEM micrograph of vertically grown layered $Co(OH)_2$ petals over rGO film, Inset shows the $Co(OH)_2$/rGO interdigitated electrodes. (b) and (c) Cyclic voltammograms of $Co(OH)_2$/rGO MSC at various scan rates. (d) Linear dependence of cathodic and anodic peak current densities with scan rate$^{1/2}$. (e) Charge–discharge curves at different current densities. (f) Cycling stability of Co $(OH)_2$/rGO and $Co(OH)_2$ MSCs over 5000 cycles at a current density of 105 μA/cm^2.

entire volume of the electrodes unlike liquid electrolyte. The cycling stability of the $Co(OH)_2$/rGO and $Co(OH)_2$/Au MSCs were tested in 1 M KOH electrolyte by continuous charging/discharging for 5000 cycles, as shown in Figure 4f. In the case of $Co(OH)_2$/rGO MSC, 77% of the capacitance was retained compared to 30% for $Co(OH)_2$ electrodes. Hence, it is clear that rGO layer enhances the capacitance of the metal oxides/hydroxides besides improving cycling stability.

Further, in order to evaluate the electrochemical performance of conducting polymer/rGO MSCs, PANI was electrodeposited over the rGO film. The electrochemical performance of PANI/rGO MSC was tested at different scan rates. As shown in Figure 5a, capacitive behavior is retained up to a scan rate of 50 V/s which is at least one order of magnitude higher than conventional devices, similar to the reported in the literature by several groups [8–10,17]. Typically, conventional devices are fabricated in sandwich configuration where the separator can be an obstacle for the free movement of electrolyte ions, unlike for the in-plane microsupercapacitors where the ion transportation happens in the same plane without having separator. Hence, in-plane devices can exhibit capacitive behavior even higher scan rates (50 V/s) when compared to the conventional devices. The charge–discharge curves of the PANI/rGO interdigital electrodes show non-linear behavior (Figure 5b), indicating the redox behavior of PANI/rGO electrodes. The cycling stability of the PANI/Au and PANI/rGO MSCs were tested as shown in Figure 5c. Similarly, PANI/rGO solid state MSCs were made by employing PVA/H_2SO_4 gel electrolyte and the electrochemical performance is shown in Figure 5d and e. Solid state device showed a volumetric capacitance of 108 F/cm^3 which is lower to that of liquid media (138 F/cm^3). It is found that the capacitance retention after 10,000 cycles is 60% for the PANI/rGO MSCs compared to 21% for PANI/Au MSCs [27]. Ragone plots of the MSCs with pseudocapacitive material/rGO electrodes are shown in Figure 5f. PANI/rGO MSC exhibits a maximum volumetric energy density of 12 mW h/cm^3 at a volumetric power density of 866 mW/cm^3. This volumetric energy density value is superior to Li-based thin-film batteries (10 mW h/cm^3), MSCs based on carbon materials (E=0.15–9 mW h/cm^3) [8–13,16–19], and metal oxides (1–5 mW h/cm^3) [19,20]. PANI/rGO MSC exhibits a maximum power density of 2800 mW/cm^3 even at an energy density of 9.3 mW h/cm^3. While $Co(OH)_2$/rGO and MnO_2/rGO MSCs exhibit maximum energy density of 6 mW h/cm^3 (at a power density of 390 mW/cm^3) and 3.4 mW h/cm^3 (at a power density of 472 mW/cm^3). Tandem configuration of PANI/rGO micro-pseudocapacitors were employed as micro-power source in glowing a red light emitting diode as shown in the inset of Figure 5f. However, we have also estimated the E_{device} and P_{device} by considering the C_{stack} values (includes total volume and area of all the components of microsupercapacitor device). We have used the following conversion factor in finding out the E_{device} and P_{device} of micro-pseudocapacitors fabricated in this study.

$$E_{device} = (1/2.25)E_{vol}$$

$$P_{device} = (1/2.25)E_{vol}$$

Please cite this article as: N. Kurra, et al., A general strategy for the fabrication of high performance microsupercapacitors, Nano Energy (2015), http://dx.doi.org/10.1016/j.nanoen.2015.05.031

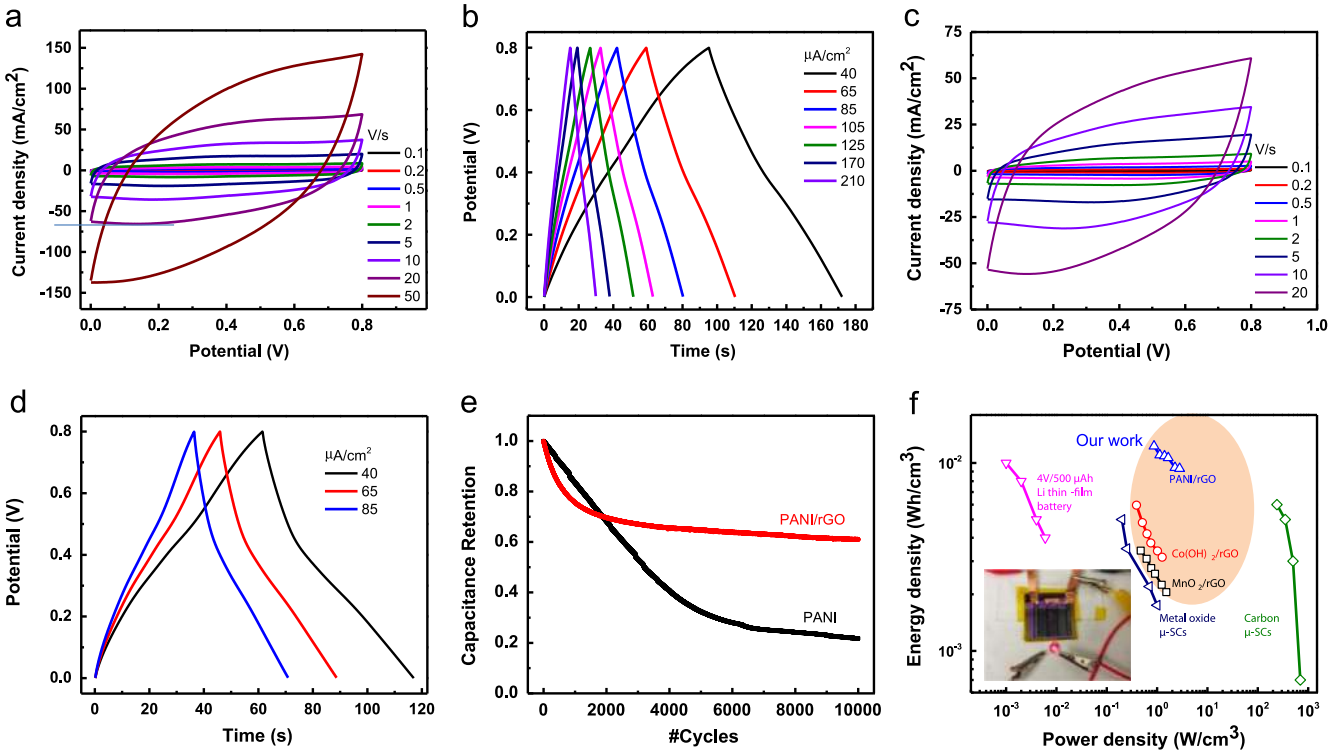

Figure 5 (a) Cyclic voltammograms of PANI/rGO MSC at various scan rates in 1 M H_2SO_4. (b) Charge–discharge profiles of PANI/rGO MSC at different current densities. (c) CVs and (d) CDs of PANI/rGO solid state MSC in PVA/H_2SO_4 gel electrolyte. (e) Cycling stability of PANI and PANI/rGO MSCs over 10,000 cycles at a current density of 105 μA/cm^2. (f) Ragone plot displaying the volumetric energy and power densities of Li thin-film batteries, carbon and metal oxide based MSCs with respect to pseudocapacitive/rGO MSCs fabricated in this study, inset shows the photograph of charged tandem PANI/rGO micro-pseudocapacitors in powering a red light emitting diode.

The volumetric energy densities are in the range of 3-12 mW h/cm^3 and power densities are in the range of 400–1200 mW/cm^3 while device energy densities are in the range of 1.3–5.3 mW h/cm^3 and power densities are in the range of 178–533 mW/cm^3. These results clearly demonstrated that the MSCs based on pseudocapacitive/rGO electrode heterostructures exhibited enhanced electrochemical stability compared to the bare pseudocapacitive materials.

Conclusions

In summary, we have demonstrated the successful fabrication of microsupercapacitors with rGO-based electrode heterostructures. Our general microfabrication strategy involves a combination of lithography and rGO transfer process, followed by pseudocapacitive material deposition. The fabricated microsupercapacitors exhibit enhanced capacitance and cycling stability compared to microsupercapacitors fabricated without the rGO layer. Our best devices, based on PANI/rGO, exhibits a maximum volumetric energy density of 12 mW h/cm^3 which is superior to current Li thin film batteries and current state-of-the-art carbon and metal oxide based microsupercapacitors, reported in the literature. Our strategy opens up new avenues in fabricating microsupercapacitors with improved electrochemical performance.

Acknowledgments

Research reported in this publication was supported by King Abdullah University of Science and Technology (KAUST). Authors thank Muhammad Shahid for useful discussions, and the Advanced Nanofabrication, Imaging and Characterization Laboratory at KAUST for their excellent support. NK acknowledges the support from SABIC Postdoctoral Fellowship.

Appendix A. Supporting information

Supplementary data associated with this article can be found in the online version at http://dx.doi.org/10.1016/j.nanoen.2015.05.031.

References

[1] P. Simon, Y. Gogotsi, Nat. Mater. 7 (2008) 845–854.
[2] Z.L. Wang, W. Wu, Angew. Chem. Int. Ed. 51 (2012) 11700–11721.
[3] F. Simjee, P.H. Chou, Proceedings of the International Symposium on Low Power Electronics and Design, ISLPED'06, 4-6 October 2006, pp. 197–202.
[4] J.W. Long, B. Dunn, D.R. Rolison, H.S. White, Chem. Rev. 104 (2004) 4463–4492.

[5] D.R. Rolison, R.W. Long, J.C. Lytle, A.E. Fischer, C.P. Rhodes, T.M. McEvoy, M.E. Bourga, A.M. Lubers, Chem. Soc. Rev. 38 (2009) 226–252.
[6] M. Beidaghi, Y. Gogotsi, Energy Environ. Sci. 7 (2014) 867–884.
[7] G. Xiong, C. Meng, R.G. Reifenberger, P.P. Irazoqui, T.S. Fisher, Electroanalysis 26 (2014) 30–51.
[8] J. Chmiola, C. Largeot, P.L. Taberna, P. Simon, Y. Gogotsi, Science 328 (2010) 480–483.
[9] D. Pech, M. Brunet, H. Durou, P. Huang, V. Mochalin, Y. Gogotsi, P.-L. Taberna, P. Simon, Nat. Nanotechnol. 5 (2010) 651–654.
[10] D. Pech, M. Brunet, P.L. Taberna, P. Simon, N. Fabre, F. Mesnilgrente, V. Con´ed´era, H. Durou, J. Power Sources (2010)1266–1269.
[11] M. Beidaghi, C.L. Wang, Adv. Funct. Mater. 22 (2012) 4501–4510.
[12] J. Lin, C. Zhang, Z. Yan, Y. Zhu, Z. Peng, R.H. Hauge, D. Natelson, J.M. Tour, Nano Lett. 13 (2012) 72–78.
[13] G. Xiong, C. Meng, R.G. Reifenberger, P.P. Irazoqui, T.S. Fisher, Energy Technol. 2 (2014) 897–905.
[14] M.D. Stoller, S. Park, Y.W. Zhu, J. An, R.S. Ruoff, Nano Lett. 8 (2008) 3498–3502.
[15] M. Shahid, N. Yesibolati, F.M. Ross, H.N. Alshareef, J. Power Sources 263 (2014) 239–245.
[16] W. Gao, N. Singh, L. Song, Z. Liu, A.L.M. Reddy, L. Ci, R. Vajtai, Q. Zhang, B. Wei, P.M. Ajayan, Nat. Nanotechnol. 6 (2011) 6–10.
[17] M.F. El-Kady, R.B. Kaner, Nat. Commun. 4 (2013) 1475.
[18] Z.S. Wu, K. Parvez, X. Feng, K. Müllen, Nat. Commun. 4 (2013) 2487.
[19] T.M. Dinh, K. Armstrong, D. Guay, D. Pech, J. Mater. Chem. A 2 (2014) 7170–7174.
[20] W. Si, C. Yan, Y. Chen, S. Oswald, L. Han, O.G. Schmidt, Energy Environ. Sci. 6 (2013) 3218–3223.
[21] N. Kurra, N.A. Alhebshi, H.N. Alshareef, Adv. Energy Mater. 4 (2014) 1401303.
[22] K. Wang, W. Zou, B. Quan, A. Yu, H. Wu, P. Jiang, Z. Wei, Adv. Energy Mater. 1 (2011) 1068–1072.
[23] C. Meng, J. Maeng, S.W.M. John, P.P. Irazoqui, Adv. Energy Mater. 4 (2014) 1301269.
[24] M. Beidaghi, C.L. Wang, Electrochim. Acta 56 (2011) 9508–9514.
[25] Z.S. Wu, G. Zhou, L.C. Yin, W. Ren, F. Li, H.M. Cheng, Nano Energy 1 (2012) 107–131.
[26] M. Zhi, C. Xiang, J. Li, M. Li, N. Wu, Nanoscale 5 (2013) 72–88.
[27] M. Xue, F. Li, J. Zhu, H. Song, M. Zhang, T. Cao, Adv. Funct. Mater. 22 (2012) 1284–1290.
[28] L.L. Peng, X. Peng, B.R. Liu, C.Z. Wu, Y. Xie, G.H. Yu, Nano Lett. 13 (2013) 2151–2157.
[29] W. Liu, C. Lu, X. Wang, R.Y. Tay, B.K. Tay, ACS Nano 9 (2015) 1528–1542.
[30] W.S. Hummers, R.E. Offeman, J. Am. Chem. Soc. 80 (1958) 1339.
[31] D. Li, M.B. Muller, S. Gilje, R.B. Kaner, G.G. Wallace, Nat. Nanotechnol. 3 (2008) 101–105.
[32] W. Chen, R.B. Rakhi, L. Hu, X. Xie, Y. Cui, H.N. Alshareef, Nano Lett. 11 (2011) 5165–5172.
[33] R.B. Rakhi, W. Chen, D. Cha, H.N. Alshareef, ACS Appl. Mater. Interfaces 6 (2014) 4196–4206.
[34] B Yao, L Yuan, X. Xiao, J. Zhang, Y. Qi, J. Zhou, J. Zhou, B. Hu, W. Chen, Nano Energy 2 (2013) 1071–1078.
[35] S. Stankovich, D.A. Dikin, R.D. Piner, K.A. Kohlhaas, A. Kleinhammes, Y. Jia, Y. Wu, S.T. Nguyen, R.S. Ruoff, Carbon 45 (2007) 15581565.
[36] F. Tuinstra, J.L. Koenig, J. Chem. Phys. 53 (1970) 1126–1130.
[37] A.C. Ferrari, J. Robertson, Phys. Rev. B 61 (2000) 14095–14107.
[38] M.A. Pimenta, G. Dresselhaus, M.S. Dresselhaus L.G. Canc,ado, A. Jorioa, R. Saito, Phys. Chem. Chem. Phys. 9 (2007) 1276–1290.
[39] E. Widjaja, J.T. Sampanthar, Anal. Chim. Acta 585 (2007) 241–245.
[40] Z. Li, J. Wang, L. Niu, J. Sun, P. Gong, W. Hong, L. Maa, S. Yang, J. Power Sources 245 (2014) 224–231.
[41] J. Jiang, L. Li, Mater. Lett. 61 (2007) 4894–4896.
[42] H.C. Liu, S. K Yen, J. Power Sources 166 (2007) 478–484.
[43] G. Cai, J. Tu, D. Zhou, J. Zhang, Q. Xiong, X. Zhao, X. Wang, C. Gu, J. Phys. Chem. C 117 (2013) 15967–15975.
[44] Y. Liu, D. Yan, R. Zhuo, S. Li, Z. Wu, J. Wang, P. Ren, P. Yan, Z. Geng, J. Power Sources 242 (2013) 78–85.
[45] C. Zhao, X. Wang, S. Wang, H. Wang, Y. Yang, W. Zheng, Mater. Res. Bull. 48 (2013) 3189–3195.
[46] U.M. Patil, M.S. Nam, J.S. Sohn, S.B. Kulkarni, R. Shin, S. Kang, S. Lee, J.H. Kim, S.C. Jun, J. Mater. Chem. A 2 (2014) 19075–190832 2 (2014) 19075–19083.

Narendra Kurra obtained his MSc degree from School of Chemistry, University of Hyderabad, India and Ph.D. from Jawaharlal Nehru Centre for Advanced Scientific Research (JNCASR), India. He is currently working as a post-doctoral fellow at King Abdullah University of Science & Technology (KAUST). His research interests include energy storage across various length scales using functional nanomaterials.

Qiu Jiang obtained his bachelor degree from University of Science and Technology of China. He is currently a Master student of the Materials Science and Engineering program at KAUST. His research interests focus on fabricating On-Chip energy storage devices employing direct write and conventional lithography techniques.

Dr. Husam Alshaeef is a Professor and Program Chairman in the Materials Science & Engineering program at King Abdullah University of Science & Technology (KAUST). He obtained his Ph.D. at North Carolina State University, USA. His group is interested in the use of nanomaterials, particularly oxides, in electronics and energy applications.

Please cite this article as: N. Kurra, et al., A general strategy for the fabrication of high performance microsupercapacitors, Nano Energy (2015), http://dx.doi.org/10.1016/j.nanoen.2015.05.031